Article

Middle–Late Pleistocene Denisovans and unresolved *Homo* in southern China

https://doi.org/10.1038/s41586-026-11341-6

Received: 2 December 2025

Accepted: 21 October 2026

Published online: 25 November 2026

Open access

Check for updates

Song Xing[1,2,15], Huiyun Rao[1,15], Guangmao Xie[3,4,15], Fan Bai[1,5,6,15], Junyi Ge[1,7], E. Andrew Bennett[1], Zhongyou Wu[1], Qingfeng Shao[8,9], Xianglei Li[1], Bence Viola[10], Qiyahui Sun[1,7], Kai Zhou[1], Zitao Li[11], Qigao Jiangzuo[1], Yuhao Zhao[12,13], Feng Liu[1], Yingjie Liu[14], Xiaotian Feng[1], Qiang Lin[4] & Qiaomei Fu[1,7] ✉

Molecular and morphological evidence increasingly supports the view that most East Asian Middle to Late Pleistocene archaic *Homo* belong to Denisovans[1], yet the presence of other contemporaneous lineages has remained unclear. Here we report a set of newly discovered hominin fossils (4 isolated teeth; more than 100.8 thousand years ago and 104.5–42.6 thousand years ago, respectively) from 2 cave sites (Chuanshandong and Longchuandong) in Guangxi, southern China. Integrated morphological and palaeoproteomic analyses reveal substantial phenotypic and molecular diversity consistent with at least two distinct lineages. One lineage (Longchuandong) is assigned to a Denisovan-affinity population, owing to its extreme similarity to Altai Denisovans with respect to dental morphology and single amino acid polymorphisms that match those of Denisovans from Harbin, Penghu, Bianfu Cave and Altai. The other lineage, represented by the Chuanshandong hominin, is an unresolved archaic *Homo*, as it carries an ancestral variant (AMELY 179M) shared with *Homo antecessor* and great apes and another variant (AMBN 253G) that is diagnostic of East Asian Middle Pleistocene *Homo erectus* but lacks the Denisovan-associated AMBN 273V variant (it being highly probable that this is inherited from *H. erectus*). Dental morphology in this lineage exhibits a mosaic of plesiomorphic and derived traits but no clear Denisovan affinity. These findings indicate that diverse hominin populations may have inhabited subtropical China during the Middle and Late Pleistocene, including a Denisovan-affinity population and another unresolved archaic *Homo*.

The taxonomic classification of East Asian late Middle Pleistocene and early Late Pleistocene hominins has been a subject of intense debate. These hominins are consistently characterized by plesiomorphic features, including a long and low neurocranium with a thick vault, a massive supraorbital torus, a sloping forehead and a robust mandible with a retreating symphysis, combined with derived traits such as an enlarged cranial capacity, a highly arched temporal squama, reduced prognathism and simplified dental morphology[2–5]. Phenotypic and molecular evidence has increasingly aligned these hominins with Denisovans[2,6–8]. For instance, the Harbin and Xujiayao crania, the Bianfu Cave radius, and the Xiahe and Penghu partial mandibles have been classified as Denisovan on the basis of palaeoproteomic and/or mitochondrial DNA analyses[1,4,6–9]. Phylogenetic studies based on trait matrices have linked Harbin Denisovans to Dali, Jinniushan, Hualongdong and Xiahe, suggesting a potentially broader distribution of Denisovans across mainland East Asia[2].

However, morphological heterogeneity persists among these hominins, for instance, cranial capacities of approximately 1,700–1,800 ml and a Neanderthal-like temporal labyrinth configuration and/or the presence of a suprainiac fossa in Xuchang and Xujiayao, and a round orbit in Maba[10–12]. Such variations have led to the proposal of distinct species, that is, pre-modern *Homo sapiens*, *Homo juluensis* and a Neanderthal-related lineage[13–17]. Moreover, most specimens attributed to the Denisovan assemblage have originated from northern and central China, with few contemporaneous hominin fossils reported from southern China, particularly subtropical regions. Thus, it remains unclear whether the East Asian late Middle Pleistocene archaic *Homo* represent only Denisovans or multiple lineages adapted to diverse environments across a vast territory.

Resolution of this question requires the discovery of more hominin fossils dating to the Denisovan period, especially from regions where such remains have not yet been reported. A comprehensive

[1]New Cornerstone Science Laboratory, Key Laboratory of Vertebrate Evolution and Human Origins, Institute of Vertebrate Paleontology and Paleoanthropology, Chinese Academy of Sciences, Beijing, China. [2]Centro Nacional de Investigación sobre la Evolución Humana (CENIEH), Burgos, Spain. [3]College of History, Culture and Tourism, Guangxi Normal University, Guilin, China. [4]Guangxi Institute of Cultural Relics Protection and Archaeology, Nanning, China. [5]Key Lab of Archaeological Sciences and Cultural Heritage, Chinese Academy of Social Sciences, Beijing, China. [6]Institute of Archaeology, Chinese Academy of Social Sciences, Beijing, China. [7]College of Earth and Planetary Sciences, University of Chinese Academy of Sciences, Beijing, China. [8]School of Geography, Nanjing Normal University, Nanjing, China. [9]Key Laboratory of Virtual Geographic Environment, Ministry of Education, Nanjing Normal University, Nanjing, China. [10]Department of Anthropology, University of Toronto, Toronto, Ontario, Canada. [11]Deerfield Academy, Deerfield, MA, USA. [12]Center for the Study of Chinese Archaeology, Peking University, Beijing, China. [13]School of Archaeology and Museology, Peking University, Beijing, China. [14]Department of Archaeology and Museology, Minzu University of China, Beijing, China. [15]These authors contributed equally: Song Xing, Huiyun Rao, Guangmao Xie, Fan Bai. ✉e-mail: fuqiaomei@ivpp.ac.cn

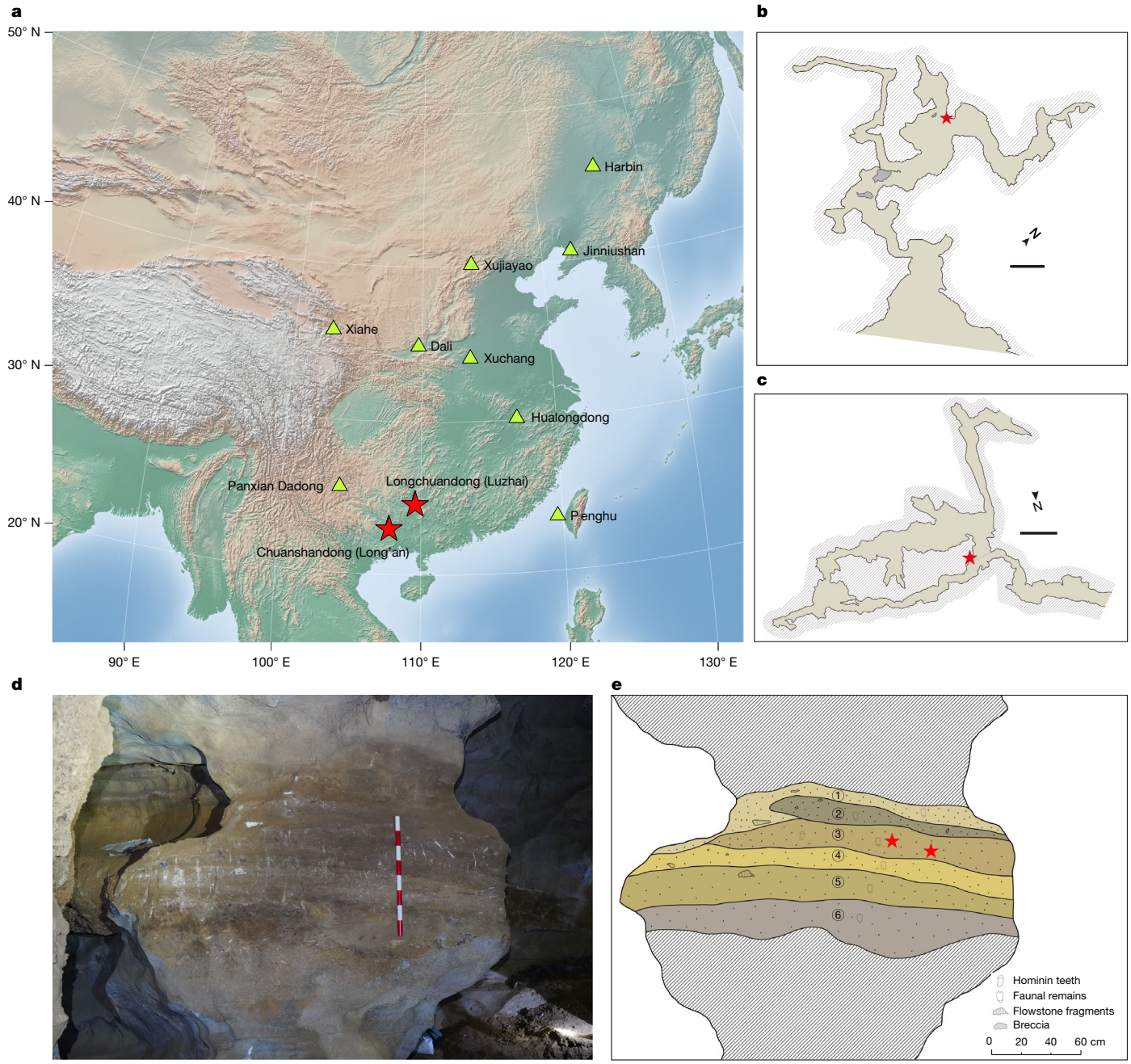


Fig. 1 | Geographical locations, plan views and stratigraphic deposition of Chuanshandong (Long'an) and/or Longchuandong (Luzhai). a, Geographical locations. **b**,**c**, Plan views of Chuanshandong in Long'an (**b**) and Longchuandong in Luzhai (**c**). **d**,**e**, Photograph (**d**) and schematic (**e**) showing stratigraphic deposition at Chuanshandong. Red stars in **a** indicate the locations of two cave sites in this study, while red stars in **b**, **c** and **e** indicate the locations where hominin teeth were recovered. Base map data in **a** from Natural Earth (https://www.naturalearthdata.com). Scale bars, 5 m (**b**), 10 m (**c**).

comparative study centred on such fossils should be conducted, incorporating a wide range of Eurasian *Homo* samples to establish a robust evolutionary framework for taxonomic identification. In addition to morphological comparisons, molecular analyses are essential for accurate taxonomic assignment. However, ancient DNA preservation is poor in the warm, humid conditions of southern China, particularly for late Middle Pleistocene specimens[4,18,19]. In such cases, palaeoproteomic analysis offers a vital complementary approach. This technology has been successfully applied to the identification of Denisovan specimens from diverse environments (including the Xiahe partial mandible[4] and rib[20] from the high-altitude Tibetan Plateau; the Penghu partial mandible[6] from the Taiwan strait; the Bianfu Cave partial parietal bones, radius and teeth[9] from southwest China; the Xujiayao cranium and mandible[1] from north China; and the Harbin cranium[7] from the plain of northeast China) and the phylogenetic placement of *Homo antecessor* (approximately 949–772 thousand years ago (ka)) and East Asian Middle Pleistocene *Homo erectus*[21,22].

A group of hominin fossils has been recovered from two sites in Nanning (Chuanshandong in Long'an County) and Liuzhou (Longchuandong in Luzhai County) within the karst terrain of Guangxi, a region renowned for its rich Pleistocene mammalian fossils, during surveys of late Middle Pleistocene cave deposits by our interdisciplinary team since 2016 (Fig. 1 and Supplementary Fig. 1). These investigations spanned an area extending more than 500 km from Chongzuo City in the southwest to Guilin City in the northeast. The discovery of these new hominin remains in this area will be critical for clarification of the

geographical distribution of Denisovans and assessment of whether multiple archaic *Homo* lineages existed in mainland East Asia during the Middle and Late Pleistocene.

Here we present direct U-series dating results for hominin teeth from Chuanshandong and Longchuandong (more than 100.8 ka and 104.5–42.6 ka, respectively), the optically stimulated luminescence (OSL) ages of the hominin fossil-bearing layer (between 49.5 ± 2.6 ka and 34.2 ± 4.1 ka) and a biostratigraphic chronology based on the faunal assemblage (late Middle to early Late Pleistocene age, younger than 300 ka). To determine the taxonomic affinity of the hominins, we performed detailed morphological descriptions and comprehensive metric and non-metric comparisons with a broader range of Eurasian *Homo* specimens. In addition, we conducted palaeoproteomic analyses of hominin teeth and compared the results with published data from *H. erectus*, *H. antecessor*, Denisovans, Neanderthals and *H. sapiens* to further clarify the taxonomic affinity of these new hominins. The integration of these approaches will enhance our knowledge of the diversity of the East Asian late Middle Pleistocene hominins.

Locations, stratigraphy and chronology

Chuanshandong lies in the karst terrain of Long'an County, Guangxi (Fig. 1). Two hominin teeth and associated abundant mammalian teeth were recovered from layer 3 of an approximately 1.2-m-thick consolidated deposit adhering to the cave walls of the western chamber entrance, the bottom deposit of which was eroded (Fig. 1, Supplementary Text 1 and Supplementary Fig. 1). The sedimentary sequence consisted of the following six layers, from top to bottom: yellowish-brown sand (layer 1), consolidated brown calcareous-cemented sand (layer 2), greyish-brown sandy silt (layer 3), yellowish-brown brecciated sand (layer 4), brown gravel-bearing clayey silt (level 5) and yellowish-brown gravel-bearing silt (level 6). The two hominin teeth were separated from each other by approximately 5 cm vertically and 20 cm horizontally within layer 3. The deposit in layer 3 consisted of homogeneous, fine-grained particles without lamination, with grain-size and size distributions similar to those of modern soil near the cave entrance. They were all polymodal, mostly dominated by the clay fraction with very low proportions of particles larger than 63 μm (less than 8.4%) and relatively low percentages of coarse fraction (Supplementary Fig. 2 and Supplementary Table 1). This suggested that the deposit of layer 3 was derived from the modern soil outside and transported by low-energy, intermittent and short-term water activity. The hominin and mammal fossils from layer 3 were dominated by isolated teeth and may have been transported gradually into the inner cave by slope gravitation resulting from a depth gradient of approximately 5 m between the cave entrance and the burial location of the teeth. Therefore, the burial age of the fossils may substantially lag behind their true age.

Longchuandong is situated in the karst landscape of Luzhai County, Guangxi (Fig. 1). Two isolated hominin teeth and numerous faunal remains were discovered in the brownish-yellow clay (Fig. 1, Supplementary Text 1 and Supplementary Fig. 1). Given that most fossils from Longchuandong are isolated teeth, the fossils were highly likely to have been sorted and transported into the deep cave by water. No stone artefacts or other cultural relics were associated with hominin fossils at these two sites.

To estimate the ages of these hominin teeth, we applied both laser-ablation-based and classic isotope-dilution-based U-series dating analyses to the hominin and associated mammalian teeth (Supplementary Text 2, Supplementary Figs. 3–5 and Supplementary Tables 2 and 3). The lower right third premolar (P_3) from Chuanshandong yielded laser ablation U-series ages ranging from 72.2 ± 1.4 ka to 63.8 ± 1.3 ka and an isotope-dilution-based age of 62.1 ± 0.3 ka. The left P_3 yielded laser ablation U-series ages ranging from 109.2 ± 2.7 ka to 97.7 ± 4.6 ka and an isotope-dilution-based U-series age of 100.8 ± 0.2 ka. These two P_3s could have originated from one individual, considering their similar morphology and degree of occlusal wear (minimum number of individuals = 1). The isotope-dilution-based U-series age of 100.8 ka thus provides a minimum age for the Chuanshandong. This age was also included in the range of the laser-ablation-based U-series ages of the associated mammal teeth (211.1–37.8 ka) (Supplementary Figs. 6–8 and Supplementary Table 4). However, the OSL ages of the hominin fossil-bearing layer in Chuanshandong ranged from 49.5 ± 2.6 ka to 34.2 ± 4.1 ka; that is, they were significantly younger than the U-series ages of the hominin teeth and most mammalian fossils, suggesting slow transportation or delayed burial of these materials (Supplementary Text 3, Supplementary Fig. 9 and Supplementary Table 5).

The upper right second molar from Longchuandong (M^2) yielded laser-ablation-based U-series ages of 46.9 ± 2.2 ka to 37.7 ± 2.0 ka and an isotope-dilution-based age of 42.6 ± 0.4 ka, whereas the lower right fourth premolar (P_4) from the same layer returned laser ablation ages of 111.0 ± 3.6 ka to 96.7 ± 3.5 ka and an isotope-dilution-based age of 104.5 ± 0.4 ka. These ages fell within the range of the laser-ablation-based U-series ages of the associated mammal teeth (160.4–30.1 ka) (Supplementary Figs. 10 and 11 and Supplementary Table 6). Associated faunal remains from both sites represented a typical *Ailuropoda-Stegodon* fauna (Supplementary Figs. 12 and 13). The presence of *Elephas maximus* and *Tapirus indicus*, together with the relatively small tooth size of *Ailuropoda* in Chuanshandong and *T. indicus* in Longchuandong, all indicate a late Middle to Late Pleistocene age (younger than 300 ka). Despite the limitations of each dating method, the integration of U-series, OSL and biostratigraphic context supports a Middle and Late Pleistocene age for the Chuanshandong and Longchuandong hominins.

Dental morphology

We described the dental morphology of a pair of P_3s from Chuanshandong and one P_4 and one M^2 from Longchuandong and compared them with a broad range of *Homo* specimens (including *H. erectus*, East Asian late Middle Pleistocene archaic *Homo*, Denisovans, Neanderthals and *H. sapiens*) to determine their taxonomy (Fig. 2 and Supplementary Tables 7–11). These materials occupied an intermediate morphological position between *H. erectus* and *H. sapiens*, characterized by a mosaic of dental traits and the absence of autapomorphic Neanderthal features. Nevertheless, the two assemblages exhibited distinct phenotypic profiles.

The first phenotypic pattern was represented by the P_4 and M^2 of Longchuandong hominins. These individuals resembled the East Asian late Middle Pleistocene archaic *Homo* with respect to both M^2 and P_4 morphology and exhibited notable affinity to Denisova 4 from Denisova Cave (Altai) in terms of M^2 characteristics (Figs. 2 and 3, Supplementary Text 4 and Supplementary Figs. 14–17). Their P_4s shared an approximately symmetrical buccal and lingual contour (unlike the mesiobuccal protruding contour typical of *H. erectus* and distolingual protruding contour typical of Neanderthals) and non-tapering roots (distinct from the tapering roots of *H. sapiens*)[3,23,24] (Supplementary Fig. 17). Their M^2s had comparable hypocone size, similar enamel–dentine junction (EDJ) shape and a non-dendritic EDJ surface, distinct from the tall crown topography and the absence of a hypocone or only ridge-like hypocone of *H. sapiens*, and from the symmetrically trapezoidal EDJ viewed occlusally and dendritic EDJ surface of *H. erectus*[23,25–31] (Fig. 3, Supplementary Fig. 15 and Supplementary Table 12). The Longchuandong M^2 did not exhibit clear variation compared with Neanderthals, especially in diffeomorphic surface matching analyses of EDJ shape (the typicality probabilities of being classified as Neanderthals were 42.13% and 39.11% in the between-group principal component analysis and canonical variate analysis, respectively), although Neanderthals tend to be characterized by a more skewed M^2 crown viewed occlusally

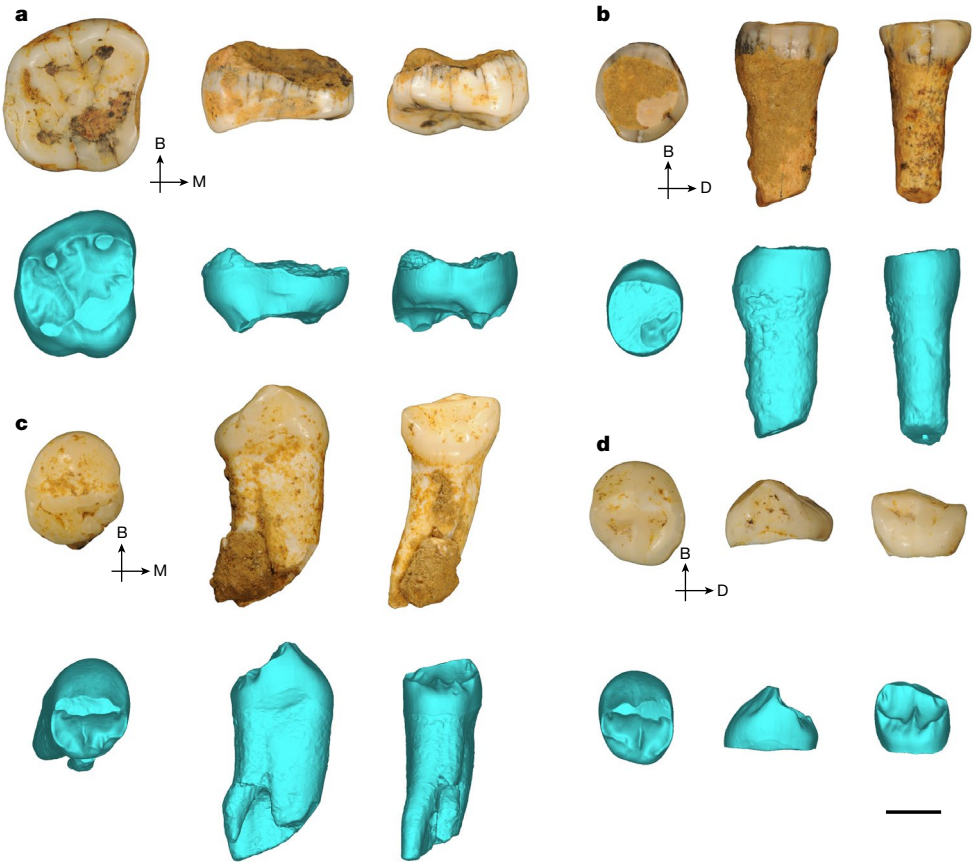


Fig. 2 | Hominin teeth from Longchuandong (Luzhai) and Chuanshandong (Long'an) and the virtual reconstruction of the enamel–dentine junction. a,**b**, Longchuandong M^2 (**a**) and Longchuandong P_4 (**b**) from Luzhai. **c**,**d**, Chuanshandong left (**c**) and right (**d**) P_3s from Long'an. The fossils and virtual reconstructions of the EDJ (shown in cyan) are displayed in the following order: occlusal, mesial and lingual views. B, buccal; M, mesial; D, distal. Scale bar, 5 mm.

and a higher occurrence of transverse crest (23.5% in early and late Neanderthals)[28,32] (Fig. 3 and Supplementary Table 12). In particular, the Longchuandong M^2 most closely resembled Denisova 4 from Denisova Cave (Altai) when all dental features analysed were considered, including the two-dimensional crown outline shape and three-dimensional EDJ shape, in addition to the crown size, relative hypocone size and degree of elevation of the crista obliqua, which overlap among different taxonomic groups to varying degrees[33–35] (Supplementary Figs. 15, 18 and 19).

The second phenotype was represented by the paired P_3s of the Chuanshandong hominin and did not align well with any established East Asian *Homo* member. These samples retained an *erectus*-like short EDJ that could be clearly distinguished from that of Neanderthals and *H. sapiens* and a complex root system with approximately constant root breadth from cervix to apex, which is normally found in *H. erectus* (for instance, the single Tomes's root with bifurcated apex in Zhoukoudian and two-rooted pattern in Sangiran) but rarely occurs in Neanderthals or *H. sapiens*[28,36–39] (Figs. 2 and 3, Supplementary Text 4, Supplementary Figs. 20–22 and Supplementary Table 13). However, the Chuanshandong P_3s exhibited derived traits that were shared with other later *Homo* and distinct from those of *H. erectus*: reduced crown asymmetry, less pronounced distolingual protrusion, a lingually displaced polygon area, absent metaconid apex (probably sharper protoconid dentine horn) and a less crenulated mesial vertical groove on the buccal surface[40,41]. They were distinguishable from the East Asian late Middle Pleistocene archaic *Homo* from Panxian Dadong, which falls within the *H. sapiens* range, with a slightly asymmetrical crown and tall EDJ topography, despite a non-tapering root[42] (Fig. 3 and Supplementary Fig. 22).

Palaeoproteomic analysis

To provide molecular evidence for taxonomy and sex attribution, we conducted ancient protein extraction on three of the hominin samples: Longchuandong M^2, Longchuandong P_4 and Chuanshandong right P_3. After searching against the Hominidae enamel database, we removed peptides that were detected in the extraction blank or attributed to contaminant proteins to control contamination from the experiment; this resulted in 2,894, 2,038 and 2,099 identified peptides for the three samples, respectively. The endogeneity of the proteome was supported by high deamidation rates of asparagine and glutamine, as well as relatively short peptide length caused by degradation (Fig. 4). We evaluated the replicate consistency by calculating the shared and specific peptide counts between two runs of liquid chromatography coupled with tandem mass spectrometry (LC–MS/MS) for each fraction from these teeth, as well as two fractions from Longchuandong P_4 (Supplementary Table 14). Although more than 50% of total peptides were shared, indicating some replicate consistency, specific peptides from each run or fraction accounted for 40% or more in total; this demonstrated the necessity of conducting multiple runs or collecting multiple fractions to improve the coverage of recovered proteome. To avoid misassignment, we removed peptides matching multiple genes, and a typical enamel-specific proteome was retrieved from the three hominin samples (Supplementary Table 15). Abundant amelogenin, Y isoform (AMELY)-specific peptides indicated that all were from male individuals. We further inspected the phylogenetically informative single amino acid polymorphisms (SAPs) to determine their population assignments by validation with BLASTp, assessment of peptide depth across three software tools, evaluation of spectral quality and quantification of

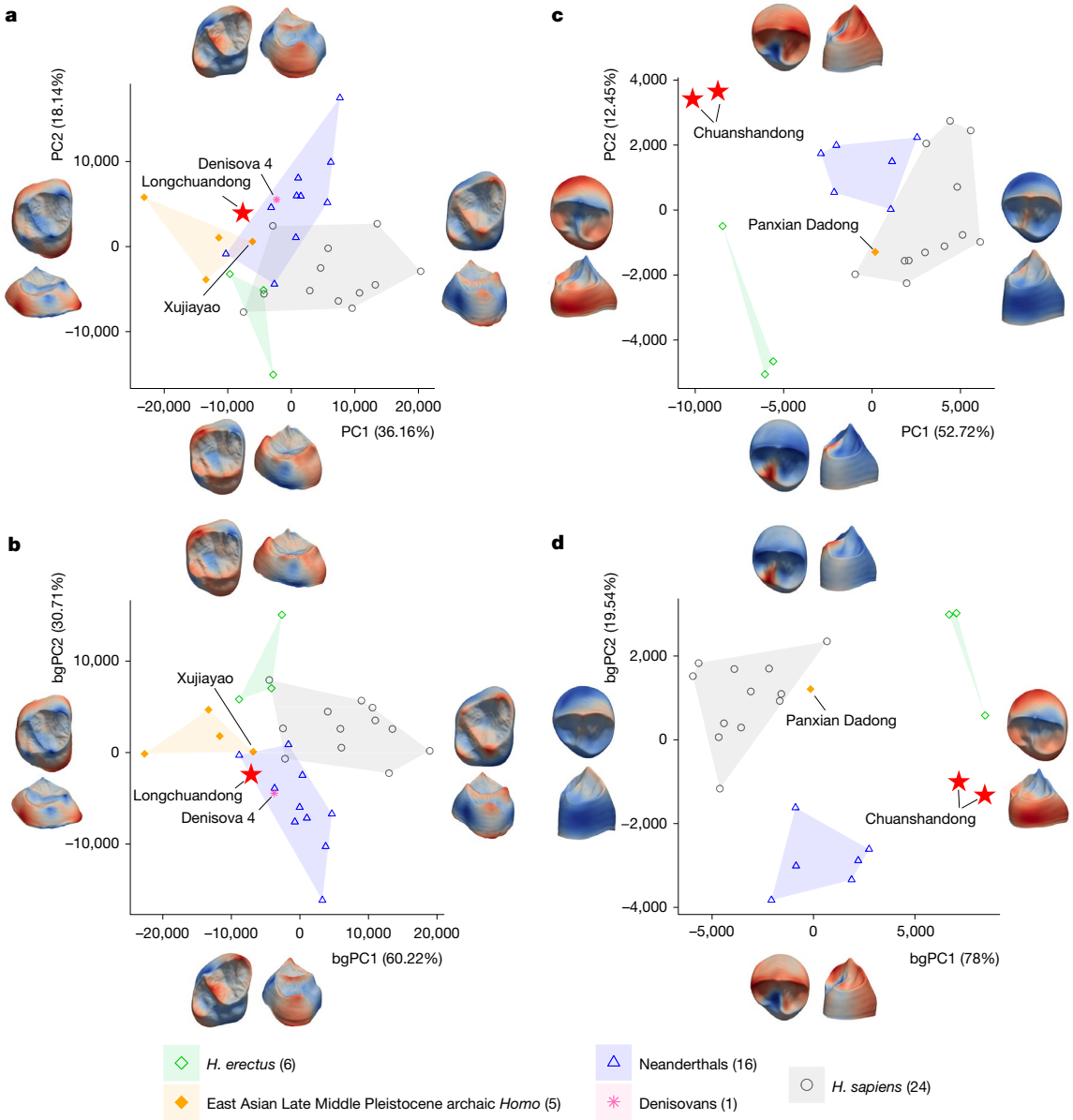


Fig. 3 | Diffeomorphic surface matching analysis of the enamel–dentine junction of the Longchuandong and Chuanshandong hominin teeth. **a**,**b**, Bivariate plots of principal component 2 (PC2) against PC1 (**a**) and between-group principal component 2 (bgPC2) against bgPC1 (**b**) based on the diffeomorphic surface matching analysis of the EDJ of the Longchuandong M^2 (Luzhai) compared with other samples. **c**,**d**, Bivariate plots of principal component 2 (PC2) against PC1 (**c**) and between-group principal component 2 (bgPC2) against bgPC1 (**d**) based on the diffeomorphic surface matching analysis of the EDJ of the two Chuanshandong P_3s (Long'an) compared with other samples. The magnitude of displacement between the global mean shape and each extreme conformation is shown as a colour map from dark blue (contracted) to red (bulged).

deamidation rates (Methods, Table 1, Supplementary Text 5, Supplementary Table 16, Supplementary Data 1 and 2 and Supplementary Figs. 23–28).

Both the Longchuandong M^2 and P_4 exhibited ameloblastin (AMBN) 273V (55 and 59 supporting peptides; Table 1), which is shared with East Asian Middle Pleistocene *H. erectus*, Harbin, Penghu, Bianfu Cave, Denisova 25 and Denisova 3, and with some *H. sapiens* from Southeast Asia and Oceania with high levels of Denisovan introgression[6,9,22,43–45]. In phylogenetic analysis, the two Longchuandong samples were grouped with Denisova 3 with 100% support (Supplementary Text 6 and Supplementary Fig. 29). Given the age of the samples and the morphological similarity between the Longchuandong M^2 and Denisova 4 from Altai Denisova Cave, the Longchuandong samples are likely to represent a Denisovan-affinity lineage in south China.

Unlike the two Longchuandong samples, Chuanshandong carried a SAP, AMBN 253G, supported by nine peptides (Table 1), among which seven peptide-spectrum matches (PSMs) had a complete series of y- and b-ions surrounding the SAP. This SAP has been reported in three groups of late *H. erectus* from Zhoukoudian, Hexian and Sunjiadong[22], but all other comparative specimens in Hominidae present AMBN 253A, including *H. antecessor* from Atapuerca[21], *H. erectus* from Dmanisi[21], Harbin[7], Penghu[6], Bianfu Cave[9], TNH2-1 from Laos[46], Denisova 3 (ref. 43), Denisova 25 (ref. 45), 9 Neanderthals[47–52], Ust'-Ishim[53], *H. sapiens* and non-human great apes. In addition, AMELY 179M, an ancestral variant that is shared with *H. antecessor*[21] and non-human great apes but not with *H. sapiens*, Neanderthals or the Denisovan clade, was also identified in Chuanshandong with seven supporting peptides (Table 1); among these, two PSMs had two b-ions bracketing the SAP, and eight PSMs had one b-ion when the SAP was located at the amino terminus. Phylogenetic analysis showed that Chuanshandong formed a sister group to the common ancestors of Neanderthals, Denisovans and *H. sapiens* (posterior probability: 100%; Supplementary Fig. 29). The

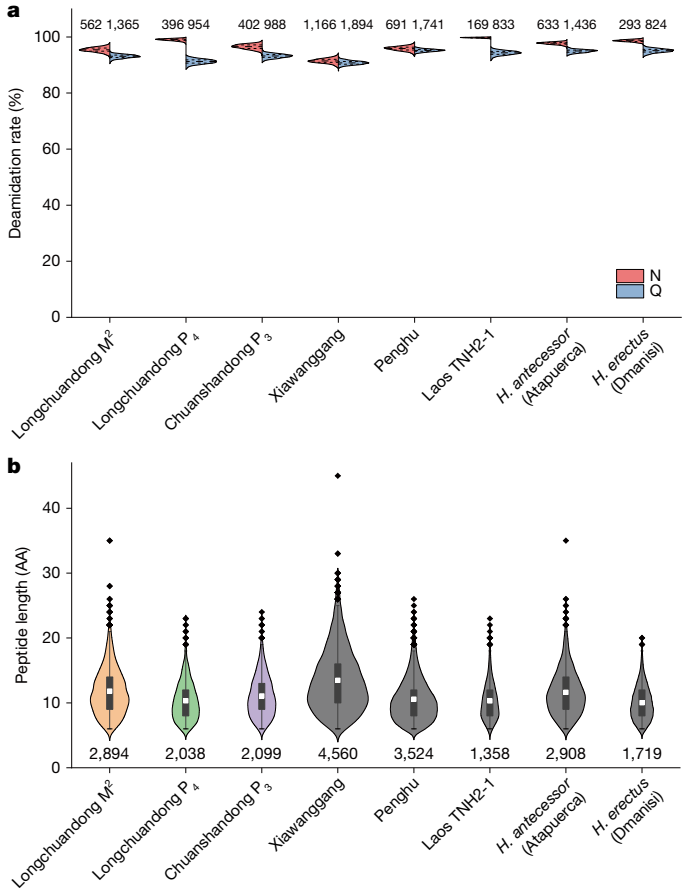


Fig. 4 | Enamel proteome degradation of the Chuanshandong and Longchuandong samples. a,**b**, Deamidation patterns (**a**) and peptide length distributions (**b**) of three hominin samples compared with the published proteome[6,21,46]. The data analysis process for published archaic individuals was the same as that used for the Chuanshandong and Longchuandong samples, except that for Laos TNH2-1, *H. antecessor* (Atapuerca) and *H. erectus* (Dmanisi), we used an expanded database with the main dentine collagens (COL1A1, COL1A2 and COL2A1). In **a**, values were derived from 1,000 bootstrap replicates of sequence deamidation. Numbers of peptides containing N or Q with valid intensity are shown for each sample. In **b**, numbers of peptides are also indicated. In **b**, box plots represent the range of the data; box edges show the lower and upper quartiles, white squares in the boxes represent median values, and whiskers extend to 1.5 times the interquartile range, with black diamonds representing outliers beyond this range.

integrated evidence indicates that Chuanshandong may belong to a lineage distinct from the Denisovan in mainland southern China.

Discussion

The scarcity of hominin fossils from subtropical southern China during the Middle to Late Pleistocene transition has hampered our understanding of the geographical distribution of Denisovans and the potential existence of other *Homo* lineages in mainland East Asia. Here we report 4 isolated hominin teeth from Guangxi (Chuanshandong and Longchuandong), dated to at least 100.8 ka and 104.5–42.6 ka, respectively. These ages establish the specimens as contemporaries of northern Denisovans (approximately 300–45 ka)[4,7,8,20,54,55] that provide important fossil evidence of non-*sapiens Homo* in subtropical regions adjacent to southeast Asia during this interval. Although both the Chuanshandong and Longchuandong hominins exhibited a mosaic of plesiomorphic and derived traits, palaeoproteomic analysis revealed variations in AMBN 253 and 273, as well in as AMELY 179, which allowed phylogenetic placement of these samples. The results indicate that at least two non-*sapiens Homo* populations may have existed in southern China's subtropics during the Middle and Late Pleistocene.

Among these diverse populations, the Longchuandong materials provide compelling evidence for the presence of a Denisovan-affinity population in subtropical southern China. Compared with *H. erectus* and *H. sapiens*, the Longchuandong more closely resembled other East Asian late Middle Pleistocene archaic *Homo*, Altai Denisova 4 and Neanderthals with respect to M^2 morphology but could be differentiated from Neanderthals by its P_4 features. These two specimens carried the AMBN 273V variant found in Harbin, Penghu, Bianfu Cave and Altai Denisovans, whereas Neanderthals and most *H. sapiens* carry the AMBN 273M variant[6,7,9,43,44,47–49,53]. These integrated morphological and molecular data together support the identification of Denisovan-affinity populations in subtropical southern China. In previous enamel proteomic studies, AMBN 273 was found to be polymorphic in Denisovans, with the M variant in Laos TNH2-1, M/V in Denisova 25 and Harbin, and V in Longchuandong, Penghu, Bianfu Cave and Denisova 3 (refs. 6,9,22,43,45,46), indicating regional variation of molecular characteristics within this lineage. Taking the Longchuandong finding into account, there is evidence that Denisovans were distributed in Siberia, northern China, the Tibetan Plateau, the Taiwan Strait, subtropical southern China and tropical Laos, suggesting their possible adaptability to diverse environments, from cold and arid high-altitude plateaus to hot and humid low-altitude regi ons[4,6–9,20,46,56,57]. Neanderthals have not been discovered in regions with confirmed Denisovan distribution other than Siberia. Given their widely separated geographical regions, the morphological similarity between Longchuandong Denisovans and Neanderthals (for instance, with respect to M^2) does not necessarily indicate hybridization. Instead, it may simply reflect the limited diagnostic value of certain anatomical features in distinguishing these two taxa. Unlike the similarity in M^2 morphology, Denisovans and Neanderthals can be effectively differentiated by other dental traits, such as the crown shape of P_4 and M^1, the labial convexity and tuberculum dentale of I^1, and other cranial and mandibular traits[1].

In contrast to Longchuandong, the remains from Chuanshandong were marked by an ancestral variant (AMELY 179M) shared with *H. antecessor* and great apes and another variant (AMBN 253G) shared with East Asian Middle Pleistocene *H. erectus* but absent from contemporaneous Denisovans, Neanderthals and *H. sapiens*. In addition, Chuanshandong retained a plesiomorphic short crown and complex roots, differing notably from Neanderthals, *H. sapiens* and the Panxian Dadong (which is considered to be potentially Denisovan on the basis of broader dental comparisons with other East Asian late Middle Pleistocene archaic *Homo*)[42]. Although Chuanshandong differed from East Asian *H. erectus* in having more progressive dental features and in the presence of AMBN 273M, the fact that they shared AMBN 253G implies that they may be related. The presence of an ancestral variant (AMELY 179M) and an *erectus*-like variant (AMBN 253G) suggests that the Chuanshandong hominin belongs to a primitive *Homo* lineage that may have survived into the Late Pleistocene in a geographical refugium. Admixture among existing archaic *Homo* in southern China or gene flow from *H. erectus* are plausible explanations for the unique molecular and morphological attributes of Chuanshandong hominin.

The findings of this study show that the subtropical area in southern China may have hosted multiple populations of archaic *Homo* during the Middle and Late Pleistocene. In addition to the previously suggested Neanderthal-related hominin at Maba in the adjacent Guangdong Province[16,17,58], we have now identified both a Denisovan-affinity hominin and another unresolved non-*sapiens* archaic *Homo* in this region. However, such phylogenetic inference based on the limited proteomic data is preliminary. More molecular data accumulated in the future, spanning broad geographical regions and time periods,

Table 1 | The details of SAPs within *Homo* identified in three hominin samples

Gene name	*AMBN*	*AMBN*	*AMELY*
UniProt ID	Q9NP70	Q9NP70	Q99218
Position	253	273	179
Longchuandong M^2 proteome	A (26,32,35)	**V** (55,49,63)	**L** (40,23,49)
Longchuandong P_4 proteome	A (19,23,30)	**V** (59,39,59)	**L** (19,9,24)
Chuanshandong P_3 proteome	**G** (9,14,17)	M (17,20,29)	M (7,4,16)
Laos TNH2-1 proteome	A (4,6,10)	M (2,3,6)	–
***H. erectus* (Dmanisi) proteome**	A	M	–
***H. antecessor* (Atapuerca) proteome**	A	M	M
East Asian *H. erectus* proteomes	**G** (*n* = 6)	**V** (*n* = 6)	–
Harbin proteome	A	M**V**	L
Penghu proteome	A	**V**	**L**
Bianfu proteomes	A (*n* = 2)	**V** (*n* = 2)	**L** (*n* = 2)
Denisova 3 genome	A	**V**	–
Denisova 25 genome	A	M**V**	**L**
Neanderthal genomes	A (*n* = 9)	M (*n* = 8)	**L** (*n* = 5)
Ust'-Ishim genome	A	M	**L**
Modern human (gnomAD)	A	M 99.993% **V** 0.007%	**L**
Great ape genomes	A	M	M

Positions were based on the UniProt accession number for the related human proteins. The derived amino acid variant is shown in bold, whereas the ancestral variant is shown in normal text. The three numbers in parentheses after the amino acid residues are the supporting peptide counts after BLASTp filtration, identified through PEAKS Online, MaxQuant and pFind, respectively. The data analysis process for Laos TNH2-1 was the same as that for the Chuanshandong and Longchuandong samples except that we used an expanded database with the main dentine collagens (COL1A1, COL1A2 and COL2A1). The listed amino acid calls for *H. erectus* from Dmanisi, East Asian *H. erectus* from Zhoukoudian, Hexian and Sunjiadong, and *H. antecessor* from Atapuerca, Harbin, Penghu and Bianfu Cave were obtained from the published protein sequences[6,9,21,22]. The amino acid residues for Denisova 3, Denisova 25, Neanderthal individuals and Ust'-Ishim were translated from genomic data[43,45,47–53]. A dash indicates that the position has not been recovered; *n* indicates the number of sequenced specimens with coverage of the position. The frequency in *H. sapiens* was obtained from the gnomAD database. Most individuals carrying derived amino acid AMBN 273V are from southeast Asia and Oceania with high Denisovan introgression[44].

and including ancient DNA from these archaic hominins, will provide us with a better understanding of the taxonomic value of specific proteomic mutations or variants and their variability between archaic and modern populations. Moreover, key diagnostic characteristics, especially trait combinations that significantly vary among different taxa, should be systematically screened from the relatively rich morphological dataset to define a lineage. Finally, it will be crucial to propose possible interpretations that can account for both morphological diversity and molecular variability, to further illustrate the framework of human evolution in East Asia.

Online content

Any methods, additional references, Nature Portfolio reporting summaries, source data, extended data, supplementary information, acknowledgements, peer review information; details of author contributions and competing interests; and statements of data and code availability are available at https://doi.org/10.1038/s41586-026-11341-6.

1. Xing, S. et al. The proteome of Middle Pleistocene Xujiayao and common Denisovan morphology. *Nature* https://doi.org/10.1038/s41586-026-11132-z (2026).
2. Ni, X. et al. Massive cranium from Harbin in northeastern China establishes a new Middle Pleistocene human lineage. *The Innovation* https://doi.org/10.1016/j.xinn.2021.100130 (2021).
3. Wu, X.-J. et al. Archaic human remains from Hualongdong, China, and Middle Pleistocene human continuity and variation. *Proc. Natl Acad. Sci. USA* **116**, 9820–9824 https://doi.org/10.1073/pnas.1902396116 (2019).
4. Chen, F. et al. A late Middle Pleistocene Denisovan mandible from the Tibetan Plateau. *Nature* **569**, 409–412 https://doi.org/10.1038/s41586-019-1139-x (2019).
5. Chang, C.-H. et al. The first archaic *Homo* from Taiwan. *Nat. Commun.* **6**, 6037 https://doi.org/10.1038/ncomms7037 (2015).
6. Tsutaya, T. et al. A male Denisovan mandible from Pleistocene Taiwan. *Science* **388**, 176–180 https://doi.org/10.1126/science.ads3888 (2025).
7. Fu, Q. et al. The proteome of the late Middle Pleistocene Harbin individual. *Science* **389**, 704–707 https://doi.org/10.1126/science.adu9677 (2025).
8. Fu, Q. et al. Denisovan mitochondrial DNA from dental calculus of the >146,000-year-old Harbin cranium. *Cell* **188**, 3919–3926 https://doi.org/10.1016/j.cell.2025.05.040 (2025).
9. Rao, H. et al. Ancient proteins identify various Denisovan remains from Southwest China. *Nature* https://doi.org/10.1038/s41586-026-10976-9 (2026).
10. Wu, X.-J. et al. Evolution of cranial capacity revisited: a view from the late Middle Pleistocene cranium from Xujiayao, China. *J. Hum. Evol.* **163**, 103119 https://doi.org/10.1016/j.jhevol.2021.103119 (2022).
11. Li, Z.-Y. et al. Late Pleistocene archaic human crania from Xuchang, China. *Science* **355**, 969–972 https://doi.org/10.1126/science.aal2482 (2017).
12. Wu, X.-J., Crevecoeur, I., Liu, W., Xing, S. & Trinkaus, E. Temporal labyrinths of eastern Eurasian Pleistocene humans. *Proc. Natl Acad. Sci. USA* **111**, 10509–10513 https://doi.org/10.1073/pnas.1410735111 (2014).
13. Wu, X. et al. Morphological description and evolutionary significance of 300 ka hominin facial bones from Hualongdong, China. *J. Hum. Evol.* **161**, 103052 https://doi.org/10.1016/j.jhevol.2021.103052 (2021).
14. Bae, C. J. & Wu, X. Making sense of eastern Asian Late Quaternary hominin variability. *Nat. Commun.* **15**, 9479 https://doi.org/10.1038/s41467-024-53918-7 (2024).
15. Bae, C. J. *The Paleoanthropology of Eastern Asia* (Univ. of Hawaii Press, 2024).
16. Wu, X. & Bruner, E. The endocranial anatomy of maba 1. *Am. J. Phys. Anthropol.* **160**, 633–643 https://doi.org/10.1002/ajpa.22974 (2016).
17. Woo, J. -k & Peng, R. -c Fossil human skull of early Paleoanthropic stage found at Mapa, Shao-quan, Kwangtung Province. *Vert. Palas.* **1**, 159–164 (1959).
18. Wang, T. et al. Human population history at the crossroads of East and Southeast Asia since 11,000 years ago. *Cell* **184**, 3829–3841 https://doi.org/10.1016/j.cell.2021.05.018 (2021).
19. Zhang, X. et al. A Late Pleistocene human genome from Southwest China. *Curr. Biol.* **32**, 3095–3109 https://doi.org/10.1016/j.cub.2022.06.016 (2022).
20. Xia, H. et al. Middle and Late Pleistocene Denisovan subsistence at Baishiya Karst Cave. *Nature* **632**, 108–113 https://doi.org/10.1038/s41586-024-07612-9 (2024).
21. Welker, F. et al. The dental proteome of *Homo antecessor*. *Nature* **580**, 235–238 https://doi.org/10.1038/s41586-020-2153-8 (2020).
22. Fu, Q. et al. Enamel proteins from six *Homo erectus* specimens across China. *Nature* **655**, 141–147 https://doi.org/10.1038/s41586-026-10478-8 (2026).
23. Wu, X. et al. The hominin teeth from the late Middle Pleistocene Hualongdong site, China. *J. Hum. Evol.* **206**, 103727 https://doi.org/10.1016/j.jhevol.2025.103727 (2025).
24. Martinón-Torres, M. et al. Hominin lower second premolar morphology: evolutionary inferences through geometric morphometric analysis. *J. Hum. Evol.* **50**, 523–533 https://doi.org/10.1016/j.jhevol.2005.12.004 (2006).
25. Xing, S. et al. Middle Pleistocene hominin teeth from Longtan Cave, Hexian, China. *PLoS ONE* **9**, e114265 https://doi.org/10.1371/journal.pone.0114265 (2014).
26. Pan, L. et al. Early Pleistocene hominin teeth from Gongwangling of Lantian, Central China. *J. Hum. Evol.* **168**, 103212 https://doi.org/10.1016/j.jhevol.2022.103212 (2022).
27. Xing, S. et al. Hominin teeth from the Middle Pleistocene site of Yiyuan, Eastern China. *J. Hum. Evol.* **95**, 33–54 https://doi.org/10.1016/j.jhevol.2016.03.004 (2016).
28. Martinón-Torres, M., Bermúdez de Castro, J. M., Gómez-Robles, A., Prado-Simón, L. & Arsuaga, J. Morphological description and comparison of the dental remains from Atapuerca-Sima de los Huesos site (Spain). *J. Hum. Evol.* **62**, 7–58 https://doi.org/10.1016/j.jhevol.2011.08.007 (2012).
29. Xing, S., Martinón-Torres, M., Bermúdez de Castro, J. M., Wu, X. & Liu, W. Hominin teeth from the early Late Pleistocene site of Xujiayao, Northern China. *Am. J. Phys. Anthropol.* **156**, 224–240 https://doi.org/10.1002/ajpa.22641 (2015).
30. He, J. Preliminary study on the teeth of Jinniushan archaic *Homo sapiens*. *Acta Anthropol. Sinica* **19** 216–256 (2000).
31. Bailey, S. E. & Liu, W. A comparative dental metrical and morphological analysis of a Middle Pleistocene hominin maxilla from Chaoxian (Chaohu), China. *Quatern. Int.* **211**, 14–23 https://doi.org/10.1016/j.quaint.2009.01.008 (2010).
32. Gómez-Robles, A., Bermúdez de Castro, J. M., Martinón-Torres, M., Prado-Simón, L. & Arsuaga, J. L. A geometric morphometric analysis of hominin upper second and third molars, with particular emphasis on European Pleistocene populations. *J. Hum. Evol.* **63**, 512–526 https://doi.org/10.1016/j.jhevol.2012.06.002 (2012).
33. Zubova, A. V., Chikisheva, T. A. & Shunkov, M. V. The morphology of permanent molars from the Paleolithic layers of Denisova Cave. *Archaeol. Ethnol. Anthropol. Eurasia* **45**, 121–134 https://doi.org/10.17746/1563-0110.2017.45.1.121-134 (2017).
34. Buzhilova, A., Derevianko, A. & Shunkov, M. The northern dispersal route: bioarchaeological data from the Late Pleistocene of Altai, Siberia. *Curr. Anthropol.* **58**, S491–S503 (2017).
35. Sawyer, S. et al. Nuclear and mitochondrial DNA sequences from two Denisovan individuals. *Proc. Natl Acad. Sci. USA* **112**, 15696–15700 (2015).
36. Weidenreich, F. The dentition of *Sinanthropus pekinensis*: a comparative odontography of the hominids. *Palaeontol. Sin. Series D* **1**, 180 (1937).
37. Kaifu, Y. et al. Taxonomic affinities and evolutionary history of the Early Pleistocene hominids of Java: dentognathic evidence. *Am. J. Phys. Anthropol.* **128**, 709–726 https://doi.org/10.1002/ajpa.10425 (2005).
38. Kallay, J. in *Dental Anthropology* (ed. Brothwell, D.) 75–86 (Pergamon, 1963).
39. Pan, L. & Zanolli, C. Comparative observations on the premolar root and pulp canal configurations of Middle Pleistocene *Homo* in China. *Am. J. Phys. Anthropol.* **168**, 637–646 https://doi.org/10.1002/ajpa.23777 (2019).

40. Gómez-Robles, A. et al. Geometric morphometric analysis of the crown morphology of the lower first premolar of hominins, with special attention to Pleistocene Homo. *J. Hum. Evol.* **55**, 627–638 https://doi.org/10.1016/j.jhevol.2008.03.011 (2008).
41. Xing, S., Martinón-Torres, M. & Bermúdez de Castro, J. M. The fossil teeth of the Peking Man. *Sci. Rep.* **8**, 2066 https://doi.org/10.1038/s41598-018-20432-y (2018).
42. Liu, W. et al. Late Middle Pleistocene hominin teeth from Panxian Dadong, South China. *J. Hum. Evol.* **64**, 337–355 https://doi.org/10.1016/j.jhevol.2012.10.012 (2013).
43. Meyer, M. et al. A high-coverage genome sequence from an archaic Denisovan individual. *Science* **338**, 222–226 https://doi.org/10.1126/science.1224344 (2012).
44. Wall, J. D. et al. The GenomeAsia 100K Project enables genetic discoveries across Asia. *Nature* **576**, 106–111 https://doi.org/10.1038/s41586-019-1793-z (2019).
45. Peyrégne, S. et al. A high-coverage genome from a 200,000-year-old Denisovan. Preprint at *bioRxiv* https://doi.org/10.1101/2025.10.20.683404 (2025).
46. Demeter, F. et al. A Middle Pleistocene Denisovan molar from the Annamite Chain of northern Laos. *Nat. Commun.* **13**, 2557 https://doi.org/10.1038/s41467-022-29923-z (2022).
47. Prüfer, K. et al. The complete genome sequence of a Neanderthal from the Altai Mountains. *Nature* **505**, 43–49 https://doi.org/10.1038/nature12886 (2014).
48. Prüfer, K. et al. A high-coverage Neandertal genome from Vindija Cave in Croatia. *Science* **358**, 655–658 https://doi.org/10.1126/science.aao1887 (2017).
49. Mafessoni, F. et al. A high-coverage Neandertal genome from Chagyrskaya Cave. *Proc. Natl Acad. Sci. USA* **117**, 15132–15136 https://doi.org/10.1073/pnas.2004944117 (2020).
50. Skov, L. et al. Genetic insights into the social organization of Neanderthals. *Nature* **610**, 519–525 https://doi.org/10.1038/s41586-022-05283-y (2022).
51. Massilani, D. et al. A high-coverage Neandertal genome from the Altai Mountains reveals population structure among Neandertals. *Proc. Natl Acad. Sci. USA* **123**, e2534576123 https://doi.org/10.1073/pnas.2534576123 (2026).
52. Hajdinjak, M. et al. Reconstructing the genetic history of late Neanderthals. *Nature* **555**, 652–656 https://doi.org/10.1038/nature26151 (2018).
53. Fu, Q. et al. Genome sequence of a 45,000-year-old modern human from western Siberia. *Nature* **514**, 445–450 https://doi.org/10.1038/nature13810 (2014).
54. Liu, W., Athreya, S., Xing, S. & Wu, X. Hominin evolution and diversity: a comparison of earlier-Middle and later-Middle Pleistocene hominin fossil variation in China. *Phil. Trans. R. Soc. B* **377**, 20210040 https://doi.org/10.1098/rstb.2021.0040 (2022).
55. Zhang, D. et al. Denisovan DNA in Late Pleistocene sediments from Baishiya Karst Cave on the Tibetan Plateau. *Science* **370**, 584–587 https://doi.org/10.1126/science.abb6320 (2020).
56. Reich, D. et al. Genetic history of an archaic hominin group from Denisova Cave in Siberia. *Nature* **468**, 1053–1060 https://doi.org/10.1038/nature09710 (2010).
57. Krause, J. et al. The complete mitochondrial DNA genome of an unknown hominin from southern Siberia. *Nature* **464**, 894–897 https://doi.org/10.1038/nature08976 (2010).
58. Hui, J., Wu, X. & Balzeau, A. Reappraisal of the morphological affinities of the Maba 1 cranium: new evidence from internal cranial anatomy. *Am. J. Biol. Anthropol.* **187**, e70064 https://doi.org/10.1002/ajpa.70064 (2025).

Publisher's note Springer Nature remains neutral with regard to jurisdictional claims in published maps and institutional affiliations.

Open Access This article is licensed under a Creative Commons Attribution-NonCommercial-NoDerivatives 4.0 International License, which permits any non-commercial use, sharing, distribution and reproduction in any medium or format, as long as you give appropriate credit to the original author(s) and the source, provide a link to the Creative Commons licence, and indicate if you modified the licensed material. You do not have permission under this licence to share adapted material derived from this article or parts of it. The images or other third party material in this article are included in the article's Creative Commons licence, unless indicated otherwise in a credit line to the material. If material is not included in the article's Creative Commons licence and your intended use is not permitted by statutory regulation or exceeds the permitted use, you will need to obtain permission directly from the copyright holder. To view a copy of this licence, visit http://creativecommons.org/licenses/by-nc-nd/4.0/.

© The Author(s) 2026

Methods

Morphological description and comparison

A sliding calliper was used to measure the mesiodistal and buccolingual dimensions of the hominin teeth, with recordings taken to the nearest 0.1 mm. We applied the terminology and grading criteria of the Arizona State University Dental Anthropology System[59], as well as the standards of Martinón-Torres et al.[28], to describe and score crown characteristics, including the hypocone size, the crista obliqua, the transverse crest of the upper molar and the transverse crest of the lower premolar. Root structures of lower premolars were scored using Wood's system[60]. The Chuanshandong and Longchuandong hominins were compared mainly with East Asian late Middle Pleistocene archaic *Homo* or Denisovans, East Asian/Southeast Asian *H. erectus*, *Homo heidelbergensis*, early and late Neanderthals and *H. sapiens*.

Two-dimensional geometric morphometric analysis

To quantify the crown contour shape, cusp and fovea arrangement, and main occlusal groove orientation of the M^2 and P_3, we conducted two-dimensional geometric morphometric analyses on the basis of occlusal photographs of the teeth oriented in anatomical position following the procedure introduced in refs. 32,40. All specimens were digitally mirrored to the same antimeres as the Chuanshandong and Longchuandong specimens in Adobe Photoshop 12.0 when they were from the opposite side. Before semilandmark placement, the interproximal wear facet was digitally restored to its original state according to the extent of wear and the profile of the neighbouring contour.

For the P_3 analysis, four landmarks were placed at the anterior fovea, posterior fovea, protoconid apex and metaconid apex. Forty equidistant semilandmarks were defined along the crown contour. For the M^2, three landmarks were placed at the intersections of the buccal and central grooves with each other and with the crown contour. These landmarks delineated four distinct curves along the crown contour and in the occlusal grooves. Each of them was divided into different and equidistant segments, and the dividing points were designated as semilandmarks. In total, 3 landmarks and 36 semilandmarks were defined on the occlusal surface of M^2.

Landmark and semilandmark coordinates were digitized using TpsDig2 v.2.12 (https://www.sbmorphometrics.org/soft-dataacq.html)[61]. Procrustes superimposition (minimizing Procrustes distances) was performed on the raw coordinates using the geomorph package (v.3.5)[62]. Principal component analysis was then conducted on the resulting shape variables. The ggplot package (v.4.0.3)[63] was used to produce a scatter plot of principal component 1 against principal component 2 for visualization of morphological variation among different taxonomic groups.

Microcomputed tomography imaging and surface reconstruction

The teeth from Chuanshandong and Longchuandong were scanned using the Phoenix V|tome|x M microfocus CT cabinet system at the Institute of Vertebrate Paleontology and Paleoanthropology, Chinese Academy of Sciences. The scanning parameters were as follows: 160 kV, 120 μA, isotropic voxel size of 34.20 μm, 0.2-mm-thick copper filter. Microcomputed tomography data of Neanderthals from Krapina were downloaded from the NESPOS database[64]. Tomographic slices in TIFF format were imported into Mimics v.17.0 (Materialise, https://www.materialise.com) for segmentation of enamel and dentine and virtual reconstruction of the pulp cavity. The resulting EDJ was exported in STL format for subsequent shape analysis. The worn dentine horn apices of Longchuandong M^2 and Chuanshandong P_3s were restored by two observers independently following a geometric method validated in previous studies in Avizo v.9.2 (https://www.thermofisher.com/amira-avizo)[65] (Supplementary Fig. 30).

Diffeomorphic surface matching of the EDJ

The three-dimensional EDJ models were imported into Avizo 9.2, and all specimens were superimposed using the 'Align Surface' function. Following superimposition, the STL files were saved and converted into VTK format using ParaView v.5.6.0 (https://www.paraview.org/). The VTK files were then read into Deformetrica v.4.3 (https://gitlab.com/icm-institute/aramislab/deformetrica) for quantification of deformations among the EDJ surfaces, modelled as diffeomorphisms[66]. Control points and momenta encoding the deformation parameters were generated and imported into R v.4.1.0 (https://www.r-project.org/)[67]. Principal component analysis, between-group principal component analysis and canonical variate analysis were performed using the following packages: RToolsForDeformetrica v.0.1 (ref. 68), ade4 v.1.7-17 (ref. 69), Morpho v.2.8 (ref. 70), gtools v.3.9.5 (ref. 71) and freesurferformats v.0.1.15 (ref. 72). Two sets of EDJ, independently reconstructed by two authors, were also analysed, and the results were compared to provide an indication of the reliability of the virtual reconstructions of the worn dentine horns (Supplementary Fig. 31).

Grain-size analysis

Six samples were collected from the fossil-bearing layer of the Chuanshandong section, as well as two samples from the modern soil near the cave entrance, for grain-size analysis. Bulk samples were first treated with 30% hydrogen peroxide to remove organic matter, followed by 10% hydrochloric acid to remove carbonates. Subsequently, the samples were dispersed with 0.5 N sodium hexametaphosphate. Grain-size was measured using a Malvern Mastersizer 3000 particle analyser with an analytical precision of less than 1%.

U-series dating

High-resolution U-series in situ analysis using laser ablation system coupled with multi-collector inductively coupled plasma mass spectrometry (LA–MC-ICP-MS) was conducted to directly date the Chuanshandong and Longchuandong hominin teeth. Laser ablation was performed using an NWRimageGEO high-energy laser ablation system (Elemental Scientific Lasers), and mass spectrometry was performed with a Neoma MC-ICP-MS system (Thermo Scientific). A high-precision MC-ICP-MS U-series dating method using solution nebulization after chromatographic separation was also applied to hominin teeth as an accuracy test. Integration of both procedures provided a minimum age for the hominins at Chuanshandong and Longchuandong. Laser-ablation-based U-series analyses were also conducted on freshly cut cross-sections of associated mammalian teeth recovered from the same stratigraphic layer within a 1-m radius of the hominin teeth (Chuanshandong). These analyses were carried out at Nanjing Normal University and the Institute of Vertebrate Paleontology and Paleoanthropology, Chinese Academy of Sciences, using the LA–MC-ICP-MS methods described in ref. 73 and the solution method described in ref. 74.

Luminescence dating

The age of the hominin teeth from Chuanshandong was constrained by optical dating of the hominin fossil-bearing sediments. Three sediment samples were collected using stainless steel tubes (20 cm long, with a diameter of 5 cm) hammered horizontally into a freshly dug vertical stratigraphic section. The tubes were immediately sealed with aluminium foil, wrapped with black plastic bags and taped to prevent light exposure and moisture loss. Sediment from the light-exposed end of each tube was separated and used for dose rate measurements, and material from the middle was used for equivalent dose (D_e) measurements. Sample preparation followed standard procedures described previously[75]. Coarse-grained quartz (90 μm to 150 μm) was extracted for D_e measurements.

Luminescence measurements were performed on a Risø Model DA-20 TL/OSL reader equipped with a $^{90}Sr/^{90}Y$ beta source for irradiation[76]

and an EMI 9235QA photomultiplier tube. Blue light-emitting diode stimulation (470 ± 30 nm) was used at 90% of 50 mW cm^{-2} full power, and 7.5 mm Hoya U-340 filters (transmission between 290 nm and 370 nm) were used for the quartz OSL measurements. The single-aliquot regenerative-dose protocol was used to determine the D_e (refs. 77,78) (Supplementary Table 17).

The uranium, thorium and potassium concentrations of the three samples were measured by inductively coupled plasma optical emission spectrometry and used to calculate the environmental dose rate. In situ water content (moist mass/dry mass) was determined by weighing samples before and after drying and assigned an absolute uncertainty of ±5%. Elemental concentrations were converted into an effective dose rate using the revised dose rate conversion factors[79] and water content attenuation factors[80]. The cosmic dose contribution was estimated on the basis of the burial depth of the sample, the thickness of the overlying cave roof (approximately 30 m), the zenith-angle dependence of cosmic rays, and the latitude, longitude and altitude of the site[81]. Final dose rates and deposition ages were calculated using DRAC[82]. Details of sample preparation, measurement and data analysis are provided in Supplementary Text 3.

Palaeoproteomic analysis

Protein extraction. Microinvasive acid etching was conducted on the tooth enamel for protein extraction, using an approach modified from a published protocol[83]. After cleaning with a disposable toothbrush, the tooth was wrapped with parafilm with the small etching region exposed. Then, the etching region was washed with 3% hydrogen peroxide for 30 s and rinsed with ultrapure water. We conducted an initial etch of 2 min by placing the etching region on to the 5% (v/v) hydrochloric acid solution in the cap of a 1.5-ml microcentrifuge tube. This etch solution was discarded. Then, a second etch of 15 min was performed twice in the cap of another microcentrifuge tube, and the etch solutions were combined. After desalting with C18 ZipTips (Thermo Fisher Scientific), the peptides were eluted into 0.1% trifluoroacetic acid in 80% acetonitrile. The eluted solution was further vacuum-evaporated before being subjected to LC–MS/MS analysis.

A Neolithic human tooth from the Xiawanggang Site (approximately 5 ka) in Henan Province, China, was chosen as a positive control sample (referred to as 'Xiawanggang'). The positive control sample and a blank extraction (negative control sample) were processed in the same batch as the hominin samples with the same protocol. All sample treatments were performed in the dedicated clean room for ancient protein analysis in the Molecular Paleontology Laboratory at the Institute of Vertebrate Paleontology and Paleoanthropology, Chinese Academy of Sciences. To evaluate the replicate consistency and improve the coverage of recovered proteome, we etched two spots on Longchuandong P_4 and obtained two fractions. Two LC–MS/MS runs were conducted for each fraction from these teeth.

Liquid chromatography–tandem mass spectrometry. The eluted peptides were analysed in data-dependent acquisition mode on an Orbitrap Exploris 480 (Thermo Fisher Scientific) interfaced with an Easy n-LC 1200 HPLC system (Thermo Scientific) at the Central Laboratory, Capital Medical University, Beijing, China. A trap column (100 μm i.d. × 2 cm, C18) and analytical column (150 μm i.d. × 15 cm, C18) were used, both packed in-house with 3 μm reversed-phase silica (Reprosil-Pur C18 AQ, Dr. Maisch GmbH). Mobile phase A was 0.1% formic acid in water, and mobile phase B was 0.1% formic acid in 80% acetonitrile. The peptides were separated using a 125-min linear gradient program (0–1 min, 1–9% B; 1–101 min, 9–28% B; 101–113 min, 28–42% B; 113–117 min, 42–99% B; 117–125 min, 99% B) at a flow rate of 350 nl min^{-1}. For the mass spectrometry, full scans were measured with a m/z range from 350 to 1,500, a resolution of 60,000, an AGC target of 300% and a maximum injection time of 50 ms. The precursors were selected for higher-energy collisional dissociation fragmentation with an isolation window of 1.6 m/z and a dynamic exclusion of 60 s. MS2 scans were obtained with a resolution of 15,000, a normalized collision energy of 30%, an AGC target of 75% and a maximum injection time of 22 ms.

Data analysis. All the raw data files from the hominin samples, as well as those from the positive and negative control samples, were searched using PEAKS Online (v.11.5)[84], MaxQuant (v.2.6.0.0)[85] and pFind (v.3.2.2)[86]. Multiple rounds of target database searching were supplemented with searching of a contaminant database used in a previous publication[7].

First, the data were searched against the entire human reference proteome downloaded from UniProt (proteome ID UP000005640, accessed on 20 May 2022) using PEAKS Online, including peptide de novo, PEAKS DB, PTM and SPIDER. The precursor ion mass tolerance and fragment ion mass tolerance were set to 10 ppm and 0.02 Da, respectively. Unspecific digestion was chosen. Deamidation (NQ), oxidation (M), hydroxylation (P), phosphorylation (STY), pyro-Glu from E and pyro-Glu from Q were set as variable modifications, and a maximum of three modifications were allowed for each peptide. The peptide length was set from 6 to 45. A false discovery rate of 1% at the spectral level was used to filter the results. Proteins were accepted if at least two peptides were present. Main enamel proteins were identified in the hominin samples, whereas no dentine-related collagens were detected. This was not unexpected, because the acid etch approach can only extract proteins from the superficial enamel and cannot access deeper layers such as dentine. Thus, dentine collagens were excluded from further analysis.

A second round of database searching was conducted using three software tools against a custom-built database, referred to as the 'Hominidae enamel database' in this study. This database was composed of sequences for 12 main enamel proteins: amelogenin, X isoform (AMELX), AMELY, AMBN, enamelin (ENAM), amelotin (AMTN), odontogenic ameloblast-associated protein (ODAM), matrix metalloproteinase 20 (MMP20), kallikrein 4 (KLK4), tuftelin (TUFT1), collagen α1(XVII) chain (COL17A1), albumin (ALB) and α2-HS-glycoprotein (AHSG). Species were restricted to Hominidae, including archaic hominins such as Denisovans and Neanderthals. Protein sequences, including canonical and isoform sequences, were downloaded from UniProt and obtained from the translated Hominid Palaeoproteomic Reference Dataset available at Zenodo[87]. Previously published protein sequences from extinct archaic hominins (*H. antecessor*, *H. erectus*, Penghu)[6,21,22], *Paranthropus*[88] and *Gigantopithecus*[89] were also incorporated. The parameters for data searching on PEAKS Online were the same as those used in the initial search against the entire human reference proteome. The parameters for MaxQuant and pFind were similar, with a few adjustments: for MaxQuant, phosphorylation (STY) was excluded from the variable modifications, the PSM and protein false discovery rates were set to 1% and 10%, respectively, and the ion tolerance and maximum number of modifications for each peptide were set to default values; and for pFind, hydroxylation (K) was also set as a variable modification, and open search was enabled. The possible mutations identified by PEAKS SPIDER and pFind open search were added to the original database for iterative data search and validation.

After removal of peptides detected in the negative control sample or assigned to contaminant proteins, we used the remaining peptides from each hominin and positive control sample to calculate deamidation profiles to support their endogeneity[90].

Validation of phylogenetically informative SAPs. After excluding SAPs that were supported by a single peptide or indistinguishable owing to post-translational modifications[7], we manually checked the variants within the *Homo* genus that met initial thresholds (PSM count ≥ 2, PSM ratio ≥ 10% and intensity ratio ≥ 10%) to confirm their reliability[6,7,88]. The criteria were as follows.

(1) BLASTp: first, all the supporting peptides were submitted to BLASTp search against the NCBInr database. Peptides that also matched

proteins from other genes or from some archaeal, bacterial or fungal species were removed from further evaluation and calculation.
(2) Depth across different software: after BLAST filtration, variants were retained for further consideration only if each software tool retained at least two peptides.
(3) MS2 support: we manually inspected the MS2 spectra of all supporting PSMs to confirm the presence of y- and b-ions around the SAP. Two levels of criteria were applied: 'MS2 support' required at least one y- or b-ion linked to the SAP, whereas 'strict MS2 support' required at least two y-ions or two b-ions bracketing the SAP. An exception was made for terminal SAPs, for which a single associated ion was accepted for the strict classification. The number of peptides meeting each criterion was then calculated.
(4) Deamidation rate: using peptides containing asparagine or glutamine residues, we calculated deamidation levels on the basis of spectral count and ion intensity. The number of PSMs and total count of covered N and Q sites were also recorded. An elevated deamidation rate in these peptides suggested an endogenous origin, which reinforced the reliability of the SAP identification.

Using these criteria, we evaluated eight positions across the three hominin samples (Supplementary Data 2) and confidently identified four of them. One of these was AMELY 59M, a male-specific SAP commonly used for sex identification[83]; details of the other three reliable SAPs are shown in Table 1.

Consensus sequence reconstruction and phylogenetic analysis. We combined the overlapping results from the three software tools and used them to generate consensus sequences for each protein from the three hominin samples with Biopython (v.1.83)[91]. For sites with more than two amino acid variants, we calculated the number of PSMs, the PSM ratio and the intensity ratio for each variant. In PEAKS Online and MaxQuant, a variant was considered to be reliable if it met all of the following thresholds: PSM count ≥ 2, PSM ratio ≥ 10% and intensity ratio ≥ 10% (ref. 7). In pFind, the intensity ratio was discarded. Confident heterozygous positions were identified as those for which multiple amino acid variants passed these filters. On the basis of the overlapping results from the three tools, no heterozygous positions were retained in the three hominin samples. Amino acid variants supported by a single peptide were excluded. The unreliable phylogenetically informative SAPs inspected above were also marked as 'X' in the consensus sequences. Finally, the consensus sequences of six proteins, AMELX, AMELY, AMBN, ENAM, COL17A1 and ALB, were reconstructed.

The comparative dataset contained four archaic individuals, five extant great ape species, a gibbon (*Nomascus leucogenys*) and a macaque (*Macaca mulatta*). The protein sequences of four archaic individuals were obtained from the Hominid Palaeoproteomic Reference Dataset[87]; these individuals comprised Denisova 3, Altai Neanderthal, Chagyrskaya 8 and Vindija33.19. Protein sequences for extant great apes and other primates were retrieved from UniProt and NCBI (Supplementary Table 18). The six proteins were aligned using MAFFT (v.7.490)[92] and concatenated with R package phylotools (v.0.2.2; https://github.com/helixcn/phylotools), resulting in a dataset with a total length of 4,108 amino acid positions. We also detected 16.67%, 14.51% and 14.68% non-missing sites in Longchuandong M^2, Longchuandong P_4 and Chuanshandong P_3, respectively. Leucines were converted into isoleucines, as these two amino acids are isobaric and were indistinguishable in the tandem mass spectrometry used in this study.

We performed phylogenetic analysis on the aligned dataset using MrBayes (v.3.2.6)[93]. The best partitioning schemes and substitution models were chosen using PartitionFinder (v.2.1.1)[94]. Two Markov chain Monte Carlo runs were performed for 10,000,000 generations, with sampling every 5,000 generations. Convergence was evaluated using the average standard deviation of split frequencies and log likelihood values. Effective sample sizes were checked using TRACER (v.1.6)[95]. After 25% burn-in, effective sample size values for all parameters were greater than 200, indicating sufficient sampling. Then, a 50% majority-rule consensus tree was constructed, with clade frequencies representing posterior probabilities.

Ethics statement

The protein analyses of the hominin specimens were approved by the Institute of Vertebrate Paleontology and Paleoanthropology, Chinese Academy of Sciences, and Guangxi Institute of Cultural Relics Protection and Archaeology. The researchers involved in the study are affiliated with these institutes.

Reporting summary

Further information on research design is available in the Nature Portfolio Reporting Summary linked to this article.

Data availability

All the proteomic mass spectrometry data are available through the ProteomeXchange Consortium via the PRIDE[96] partner repository (accession no. PXD071210). Protein consensus sequences for the Chuanshandong and Longchuandong individuals used for phylogenetic analysis are available in Supplementary Data 3 and details of the phylogenetic analysis carried out in MrBayes are provided in Supplementary Data 4. Reference palaeoproteomic data are available through the PRIDE partner repository with dataset identifiers PXD054412 (Penghu specimen), PXD014342 (Dmanisi *H. erectus* specimen D4163 and Atapuerca *H. antecessor* specimen ATD6-92) and PXD018721 (Laos TNH2-1 specimen). The Hominid Palaeoproteomic Reference Dataset is available at Zenodo (https://doi.org/10.5281/zenodo.7728060)[87]. All other reference protein sequences are available from the UniProt Knowledgebase (https://www.uniprot.org/) and the National Center for Biotechnology Information (https://www.ncbi.nlm.nih.gov/). The 3D data of hominin teeth from Chuanshandong and Longchuandong are available in MorphoSource (https://www.morphosource.org) under Media IDs 000923198, 000923147, 000923166, 000923172, 000923177, 000923183, 000923188 and 000923193. The worldwide base maps of land, ocean and rivers are available from Natural Earth (https://www.naturalearthdata.com/).

59. Turner II, C. G., Nichol, C. R. & Scott, G. R. in *Advances in Dental Anthropology* (eds M. Kelley & C. Larsen) 13–31 (Wiley-Liss, 1991).
60. Wood, B. A., Abbott, S. A. & Uytterschaut, H. Analysis of the dental morphology of Plio-Pleistocene hominids. IV. Mandibular postcanine root morphology. *J. Anat.* **156**, 107–139 (1988).
61. Rohlf, F. J. TpsDig2 https://www.sbmorphometrics.org/soft-dataacq.html (1998).
62. Adams, D. C., Collyer, M. & Kaliontzopoulou, A. Geomorph: software for geometric morphometric analyses. R package version 3.2.1 https://cran.r-project.org/package=geomorph (2020).
63. Wickham, H. *ggplot2: elegant graphics for data analysis* (Springer-Verlag, 2016).
64. NESPOS database. Neanderthal Studies Professional Online Service. https://archiv.neanderthal.de/data/ (2019).
65. Zanolli, C. et al. The Middle Pleistocene (MIS 12) human dental remains from Fontana Ranuccio (Latium) and Visogliano (Friuli-Venezia Giulia), Italy. A comparative high resolution endostructural assessment. *PLoS ONE* **13**, e0189773 https://doi.org/10.1371/journal.pone.0189773 (2018).
66. Bône, A., Louis, M., Martin, B. & Durrleman, S. in *Shape in Medical Imaging* (eds Martin Reuter et al.) 3–13 (Springer, 2018).
67. R Core Team *R: A Language and Environment for Statistical Computing* (R Foundation for Statistical Computing, 2021).
68. Dumoncel, J. Tools for Deformetrica. *GitLab* https://gitlab.com/jeandumoncel/tools-for-deformetrica/Tools for Deformetrica (2021).
69. Dray, S. & Dufour, A.-B. The ade4 package: implementing the duality diagram for ecologists. *J. Stat. Softw.* **22**, 1–20 (2007).
70. Schlager, S., Jefferis, G. & Dryden, I. Morpho: calculations and visualisations related to geometric morphometrics. *GitHub* https://github.com/zarquon42b/Morpho (2017).
71. Warnes, G. et al. gtools: various R programming tools. *GitHub* https://github.com/r-gregmisc/gtools (2023)
72. Schäfer, T. freesurferformats: read and write 'FreeSurfer' neuroimaging file formats. *GitHub* https://github.com/dfsp-spirit/freesurferformats (2026).
73. Liu, Y., Jiao, Y. N., Lu, Z. Z., Hu, G. L. & Shao, Q. F. U-series in situ dating of fossils using LA-MC-ICPMS. *Acta Anthropol. Sinica* **44**, 700–713 (2025).

74. Shao, Q. et al. Interactive programs of MC-ICPMS data processing for 230Th/U geochronology. *Quat. Geochronol.* https://doi.org/10.1016/J.QUAGEO.2019.01.004 (2019).
75. Jacobs, Z. et al. Timing of archaic hominin occupation of Denisova Cave in southern Siberia. *Nature* **565**, 594–599 https://doi.org/10.1038/s41586-018-0843-2 (2019).
76. Bøtter-Jensen, L., Andersen, C. E., Duller, G. A. T. & Murray, A. S. Developments in radiation, stimulation and observation facilities in luminescence measurements. *Radiat. Meas.* **37**, 535–541 https://doi.org/10.1016/S1350-4487(03)00020-9 (2003).
77. Murray, A. S. & Wintle, A. G. The single aliquot regenerative dose protocol: potential for improvements in reliability. *Radiat. Meas.* **37**, 377–381 https://doi.org/10.1016/S1350-4487(03)00053-2 (2003).
78. Murray, A. S. & Wintle, A. G. Luminescence dating of quartz using an improved single-aliquot regenerative-dose protocol. *Radiat. Meas.* **32**, 57–73 https://doi.org/10.1016/S1350-4487(99)00253-X (2000).
79. Guérin, G., Mercier, N. & Adamiec, G. Dose-rate conversion factors: update. *Ancient TL* **29**, 5–8 https://doi.org/10.26034/la.atl.2011.443 (2011).
80. Aitken, M. J. *Thermoluminescence Dating* (Academic, 1985).
81. Prescott, J. R. & Hutton, J. T. Cosmic ray contributions to dose rates for luminescence and ESR dating: Large depths and long-term time variations. *Radiat. Meas.* **23**, 497–500 https://doi.org/10.1016/1350-4487(94)90086-8 (1994).
82. Durcan, J. A., King, G. E. & Duller, G. A. T. DRAC: dose rate and age calculator for trapped charge dating. *Quat. Geochronol.* **28**, 54–61 https://doi.org/10.1016/j.quageo.2015.03.012 (2015).
83. Stewart, N. A., Gerlach, R. F., Gowland, R. L., Gron, K. J. & Montgomery, J. Sex determination of human remains from peptides in tooth enamel. *Proc. Natl Acad. Sci. USA* **114**, 13649–13654 https://doi.org/10.1073/pnas.1714926115 (2017).
84. Xin, L. et al. A streamlined platform for analyzing tera-scale DDA and DIA mass spectrometry data enables highly sensitive immunopeptidomics. *Nat. Commun.* **13**, 3108 https://doi.org/10.1038/s41467-022-30867-7 (2022).
85. Cox, J. & Mann, M. MaxQuant enables high peptide identification rates, individualized p.p.b.-range mass accuracies and proteome-wide protein quantification. *Nat. Biotechnol.* **26**, 1367–1372 https://doi.org/10.1038/nbt.1511 (2008).
86. Shao, G. et al. How to use open-pFind in deep proteomics data analysis?—A protocol for rigorous identification and quantitation of peptides and proteins from mass spectrometry data. *Biophys. Rep.* **7**, 207–226 https://doi.org/10.52601/bpr.2021.210004 (2021).
87. Patramanis, I., Ramos Madrigal, J., Cappellini, E. & Racimo, F. Hominid Palaeoproteomic Reference Dataset. *Zenodo* https://doi.org/10.5281/zenodo.7728060 (2022).
88. Madupe, P. P. et al. Enamel proteins reveal biological sex and genetic variability in southern African *Paranthropus*. *Science* **388**, 969–973 https://doi.org/10.1126/science.adt9539 (2025).
89. Welker, F. et al. Enamel proteome shows that *Gigantopithecus* was an early diverging pongine. *Nature* **576**, 262–265 https://doi.org/10.1038/s41586-019-1728-8 (2019).
90. Mackie, M. et al. Palaeoproteomic profiling of conservation layers on a 14th century Italian wall painting. **57**, 7369–7374 https://doi.org/10.1002/anie.201713020 (2018).
91. Cock, P. J. et al. Biopython: freely available Python tools for computational molecular biology and bioinformatics. *Bioinformatics* **25**, 1422–1423 https://doi.org/10.1093/bioinformatics/btp163 (2009).
92. Katoh, K. & Standley, D. M. MAFFT multiple sequence alignment software version 7: improvements in performance and usability. *Mol. Biol. Evol.* **30**, 772–780 https://doi.org/10.1093/molbev/mst010 (2013).
93. Ronquist, F. et al. MrBayes 3.2: efficient Bayesian phylogenetic inference and model choice across a large model space. *Syst. Biol.* **61**, 539–542 https://doi.org/10.1093/sysbio/sys029 (2012).
94. Lanfear, R., Frandsen, P. B., Wright, A. M., Senfeld, T. & Calcott, B. PartitionFinder 2: new methods for selecting partitioned models of evolution for molecular and morphological phylogenetic analyses. *Mol. Biol. Evol.* **34**, 772–773 https://doi.org/10.1093/molbev/msw260 (2017).
95. Rambaut, A. & Drummond, A. J. Tracer v1.6 https://tree.bio.ed.ac.uk/software/tracer (2013).
96. Perez-Riverol, Y. et al. The PRIDE database at 20 years: 2025 update. *Nucleic Acids Res.* **53**, D543–D553 https://doi.org/10.1093/nar/gkae1011 (2025).

Acknowledgements We thank Z. Zou and S. Tang for visualization of Fig. 4 and Supplementary Figs. 23–28; M. Martinón-Torres for permission to use photographs of Atapuerca Sima de los Huesos teeth for two-dimensional geometric morphometric analyses; X. Wu for permitting the inclusion of Hualongdong teeth during the morphological comparison; and Q. Chen, S. Min and J. Ma for recording the coordinates used to draw the plane map of the cave. We also thank the NESPOS Society for sharing microcomputed tomography data for Krapina teeth.

Author contributions Q.F. designed and supervised the research project. S.X., G.X. and Q.L. supervised the field work. S.X., H.R., F.B., J.G., E.A.B., Z.W., Q. Shao, X.L., Q. Sun, Z.L., Q.J., Y.Z., X.F. and Q.F. analysed data. S.X., H.R., J.G., Q. Shao, B.V. and Q.F. prepared the database. H.R., J.G., Q. Shao, X.L., K.Z., F.L. and Q.F. performed or supervised laboratory work. S.X., H.R., J.G., Q. Shao, Q.J. and Q.F. wrote the manuscript. Q.F. revised the manuscript. S.X., H.R., J.G., Q. Shao, X.L., Q. Sun., Y.Z., Y.L. and Q.F. wrote and prepared the supplementary information. All authors discussed and critically revised the manuscript and approved the final version.

Funding This work was supported by the National Natural Science Foundation of China (L2424324), the Archaeological Talent Promotion Program of China (2024–278), the New Cornerstone Science Foundation, the National Natural Science Foundation of China (42472249 and 42372011) and the Major Program of National Social Science Foundation of China (22& ZD246).

Competing interests The authors declare no competing interests.

Additional information

Supplementary information The online version contains supplementary material available at https://doi.org/10.1038/s41586-026-11341-6.

Correspondence and requests for materials should be addressed to Qiaomei Fu.

Peer review information *Nature* thanks Maxime Aubert, Fabrice Demeter, Laura Martín-Francés and the other, anonymous, reviewer(s) for their contribution to the peer review of this work. Peer reviewer reports are available.

Reprints and permissions information is available at http://www.nature.com/reprints.

nature portfolio

Corresponding author(s): Qiaomei Fu

Last updated by author(s): Oct 12, 2026

Reporting Summary

Nature Portfolio wishes to improve the reproducibility of the work that we publish. This form provides structure for consistency and transparency in reporting. For further information on Nature Portfolio policies, see our Editorial Policies and the Editorial Policy Checklist.

Statistics

For all statistical analyses, confirm that the following items are present in the figure legend, table legend, main text, or Methods section.

n/a	Confirmed
☐	☒ The exact sample size (*n*) for each experimental group/condition, given as a discrete number and unit of measurement
☐	☒ A statement on whether measurements were taken from distinct samples or whether the same sample was measured repeatedly
☒	☐ The statistical test(s) used AND whether they are one- or two-sided *Only common tests should be described solely by name; describe more complex techniques in the Methods section.*
☒	☐ A description of all covariates tested
☒	☐ A description of any assumptions or corrections, such as tests of normality and adjustment for multiple comparisons
☐	☒ A full description of the statistical parameters including central tendency (e.g. means) or other basic estimates (e.g. regression coefficient) AND variation (e.g. standard deviation) or associated estimates of uncertainty (e.g. confidence intervals)
☒	☐ For null hypothesis testing, the test statistic (e.g. *F*, *t*, *r*) with confidence intervals, effect sizes, degrees of freedom and *P* value noted *Give P values as exact values whenever suitable.*
☐	☒ For Bayesian analysis, information on the choice of priors and Markov chain Monte Carlo settings
☒	☐ For hierarchical and complex designs, identification of the appropriate level for tests and full reporting of outcomes
☒	☐ Estimates of effect sizes (e.g. Cohen's *d*, Pearson's *r*), indicating how they were calculated

Our web collection on statistics for biologists contains articles on many of the points above.

Software and code

Policy information about availability of computer code

Data collection	No software was used for data collection.
Data analysis	All software packages used for analysis are cited in the Methods section and all used packages are publicly available: PEAKS Online: https://www.bioinfor.com/peaks-online, version: 11.5 MaxQuant: https://maxquant.org, version: 2.6.0.0 pFind: https://pfind.ict.ac.cn, version: 3.2.2 deamidation: https://github.com/dblyon/deamidation, commit: c572dcf BLAST: https://ftp.ncbi.nlm.nih.gov/blast/executables/blast+/2.15.0, version: 2.15.0 Biopython: https://biopython.org, version: 1.83 MAFFT: https://github.com/Schaudge/MAFFT, version: 7.490 phylotools: https://github.com/helixcn/phylotools, version: 0.2.2 Tracer: https://tree.bio.ed.ac.uk/software/tracer, version: 1.6 Partition Finder: http://www.robertlanfear.com/partitionfinder, version: 2.1.1 Mrbayes: https://nbisweden.github.io/MrBayes, version: 3.2.6 x64 Mimics: https://www.materialise.com, version: 17.0 Avizo: https://www.thermofisher.com/amira-avizo, version: 9.2 Deformetrica: https://gitlab.com/icm-institute/aramislab/deformetrica, version: 4.3 R: https://www.r-project.org/ version: 4.1.0 TpsDig2: https://www.sbmorphometrics.org/soft-dataacq.html, version: 2.12 ParaView: https://www.paraview.org, version: 5.6.0 geomorph: https://CRAN.R-project.org/package=geomorph, version: 3.5

ggplot: https://ggplot2.tidyverse.org, version: 4.0.3
RToolsForDeformetrica: https://gitlab.com/jeandumoncel/tools-for-deformetrica/, version: 0.1
ade4: https://CRAN.R-project.org/package=ade4, version: 1.7-17
Morpho: https://CRAN.R-project.org/package=Morpho, version: 2.8
gtools: https://CRAN.R-project.org/package=gtools, version: 3.9.5
freesurferformats: https://CRAN.R-project.org/package=freesurferformats, version: 0.1.15

For manuscripts utilizing custom algorithms or software that are central to the research but not yet described in published literature, software must be made available to editors and reviewers. We strongly encourage code deposition in a community repository (e.g. GitHub). See the Nature Portfolio guidelines for submitting code & software for further information.

Data

Policy information about availability of data

All manuscripts must include a data availability statement. This statement should provide the following information, where applicable:

- Accession codes, unique identifiers, or web links for publicly available datasets
- A description of any restrictions on data availability
- For clinical datasets or third party data, please ensure that the statement adheres to our policy

All the proteomic mass spectrometry data are available through the ProteomeXchange Consortium via the PRIDE partner repository (accession no. PXD071210). Protein consensus sequences for the Chuanshandong and Longchuandong individuals used for phylogenetic analysis are available in Supplementary Data 3, and the details of phylogenetic analysis carried out in MrBayes are provided in Supplementary Data 4.

Research involving human participants, their data, or biological material

Policy information about studies with human participants or human data. See also policy information about sex, gender (identity/presentation), and sexual orientation and race, ethnicity and racism.

Reporting on sex and gender	NA
Reporting on race, ethnicity, or other socially relevant groupings	NA
Population characteristics	NA
Recruitment	NA
Ethics oversight	NA

Note that full information on the approval of the study protocol must also be provided in the manuscript.

Field-specific reporting

Please select the one below that is the best fit for your research. If you are not sure, read the appropriate sections before making your selection.

☐ Life sciences ☐ Behavioural & social sciences ☒ Ecological, evolutionary & environmental sciences

For a reference copy of the document with all sections, see nature.com/documents/nr-reporting-summary-flat.pdf

Ecological, evolutionary & environmental sciences study design

All studies must disclose on these points even when the disclosure is negative.

Study description	Proteomic analysis of the Middle-Late Pleistocene teeth specimens
Research sample	Teeth
Sampling strategy	protein extraction
Data collection	All the pretreatment of the sample were conducted by the technicians at the Key Laboratory of Vertebrate Evolution and Human Origins, Institute of Vertebrate Paleontology and Paleoanthropology (IVPP), Chinese Academy of Sciences (CAS). And the LC MS/MS analysis was conducted by technicians in Central Laboratory (Capital Medical University).
Timing and spatial scale	~101ka, 126ka, southern China
Data exclusions	No data was excluded during the study.
Reproducibility	Replicate runs were conducted on LC MSMS analysis. These results can be cross-validated.

Randomization	Randomization was not relevant to this study.
Blinding	Blinding was not relevant to this study.

Did the study involve field work? ☒ Yes ☐ No

Field work, collection and transport

Field conditions	subtropical area, southern China
Location	107.77°E, 22.46°N; 109.55°E, 24.64°N; 107.74°E, 23.01°N
Access & import/export	Institute of Vertebrate Paleontology and Paleoanthropology, Chinese Academy of Sciences and Guangxi Institute of Cultural Relics Protection and Archaeology work together to recover the materials during field investigation.
Disturbance	The field work doesn't cause disturbance.

Reporting for specific materials, systems and methods

We require information from authors about some types of materials, experimental systems and methods used in many studies. Here, indicate whether each material, system or method listed is relevant to your study. If you are not sure if a list item applies to your research, read the appropriate section before selecting a response.

Materials & experimental systems

n/a	Involved in the study
☒	☐ Antibodies
☒	☐ Eukaryotic cell lines
☐	☒ Palaeontology and archaeology
☒	☐ Animals and other organisms
☒	☐ Clinical data
☒	☐ Dual use research of concern
☒	☐ Plants

Methods

n/a	Involved in the study
☒	☐ ChIP-seq
☒	☐ Flow cytometry
☒	☐ MRI-based neuroimaging

Palaeontology and Archaeology

Specimen provenance	Permission was granted to Qiaomei Fu of the IVPP,CAS for the sampling of the specimens for molecular analyses.
Specimen deposition	Institute of Vertebrate Paleontology and Paleoanthropology, Chinese Academy of Sciences, Guangxi Institute of Cultural Relics Protection and Archaeology
Dating methods	The specimens are dated by U-series

☒ Tick this box to confirm that the raw and calibrated dates are available in the paper or in Supplementary Information.

Ethics oversight	The protein analyses on the hominin specimens were approved by Institute of Vertebrate Paleontology and Paleoanthropology, Chinese Academy of Sciences and Guangxi Institute of Cultural Relics Protection and Archaeology. Researchers from these institutes have been affiliated.

Note that full information on the approval of the study protocol must also be provided in the manuscript.

Plants

Seed stocks	*Report on the source of all seed stocks or other plant material used. If applicable, state the seed stock centre and catalogue number. If plant specimens were collected from the field, describe the collection location, date and sampling procedures.*
Novel plant genotypes	*Describe the methods by which all novel plant genotypes were produced. This includes those generated by transgenic approaches, gene editing, chemical/radiation-based mutagenesis and hybridization. For transgenic lines, describe the transformation method, the number of independent lines analyzed and the generation upon which experiments were performed. For gene-edited lines, describe the editor used, the endogenous sequence targeted for editing, the targeting guide RNA sequence (if applicable) and how the editor was applied.*
Authentication	*Describe any authentication procedures for each seed stock used or novel genotype generated. Describe any experiments used to assess the effect of a mutation and, where applicable, how potential secondary effects (e.g. second site T-DNA insertions, mosiacism, off-target gene editing) were examined.*